vibration

MDPI

Article

A Time-Domain Solution Method for the Vibration Performance of Viscoelastic Functionally Graded Porous Beams

Yuhua Cui [1], Tao Zeng [1,2,3,4,*], Yipeng Yang [1], Xiaohong Wang [1,2,3], Guodong Xu [1,2,3] and Su Cheng [1,5]

[1] Department of Civil Engineering and Smart Cities, Shantou University, Shantou 515063, China; 19yhcui@stu.edu.cn (Y.C.); 21ypyang@stu.edu.cn (Y.Y.); xiaohongwang@stu.edu.cn (X.W.); xuguodong@stu.edu.cn (G.X.); chengsu2002@163.com (S.C.)
[2] Special Ceramics Advanced Manufacturing Engineering Technology Research Center of Guangdong Provincial University, Shantou University, Shantou 515063, China
[3] Engineering and Technology Research Centre of Advanced Composite Materials and Structures Advanced Manufacturing, Shantou University, Shantou 515063, China
[4] Intelligent Manufacturing Key Laboratory of Ministry of Education, Shantou University, Shantou 515063, China
[5] School of Civil Engineering and Architecture, Harbin University of Science and Technology, Harbin 150080, China
* Correspondence: taozeng@hrbust.edu.cn

Abstract: The viscoelastic behavior of functionally graded (FG) materials significantly affects their vibration performance, making it necessary to establish theoretical analysis methods. Although fractional-order methods can be used to set up the vibration differential equations for viscoelastic, functionally graded beams, solving these fractional differential equations typically involves complex iterative processes, which makes the vibration performance analysis of viscoelastic FG materials challenging. To address this issue, this paper proposes a simple method to predict the vibration behavior of viscoelastic FG beams. The fractional viscoelastic, functionally graded porous (FGP) beam is modeled based on the Euler–Bernoulli theory and the Kelvin–Voigt fractional derivative stress-strain relation. Employing the variational principle and the Hamilton principle, the partial fractional differential equation is derived. A method based on Bernstein polynomials is proposed to directly solve fractional vibration differential equations in the time domain, thereby avoiding the complex iterative procedures of traditional methods. The viscoelastic, functionally graded porous beams with four porosity distributions and four boundary conditions are investigated. The effects of the porosity coefficient, pore distribution, boundary conditions, fractional order, and viscoelastic coefficient are analyzed. The results show that this is a feasible method for analyzing the viscoelastic behavior of FGP materials.

Keywords: functionally graded beams; vibration; viscoelastic behavior; fractional differential equations; Bernstein polynomials

check for updates

Academic Editors: Neil G. Stephen and Aleksandar Pavic

Received: 29 April 2025
Revised: 19 May 2025
Accepted: 27 May 2025
Published: 29 May 2025

Citation: Cui, Y.; Zeng, T.; Yang, Y.; Wang, X.; Xu, G.; Cheng, S. A Time-Domain Solution Method for the Vibration Performance of Viscoelastic Functionally Graded Porous Beams. *Vibration* **2025**, *8*, 28. https://doi.org/10.3390/vibration8020028

Copyright: © 2025 by the authors. Licensee MDPI, Basel, Switzerland. This article is an open access article distributed under the terms and conditions of the Creative Commons Attribution (CC BY) license (https://creativecommons.org/licenses/by/4.0/).

1. Introduction

Functionally graded materials can smoothly transition their mechanical properties, effectively reducing internal stress concentrations and enhancing the durability and performance of the overall structure [1]. Functionally graded porous materials, a subset of FG materials, are characterized by numerous interior pores that can form during the sintering process or be intentionally introduced in specific distribution patterns. The unique characteristics of FGP materials, which are directly influenced by the shape and distribution of these interior pores, result in exceptional mechanical, thermal, chemical, biological,

and electrical properties [2]. These properties make FGP materials widely applicable in aerospace and other engineering fields. In these fields, vibration of materials and structures is quite common. Therefore, studying the vibration characteristics of FGP materials is very important, as it directly affects the stability and lifespan of equipment [3,4].

In the past few decades, many researchers have proposed a large number of beam theories, such as Euler beam theory [5–9], first-order shear deformation theory [10], and higher-order shear deformation theory [11–13], to analyze the vibration performance of FGP materials. Alnujaie et al. [14] investigated the damped forced vibration of layered FG thick beams by utilizing the finite element method and Lagrange's equations. Wu et al. [15] investigated the nonlinear forced vibrations of beams, made of porous materials with bidirectional functional gradients, using the Galerkin method. Lei et al. [16] investigated the dynamic behaviors of single-span and multi-span FGP beams with flexible boundary constraints using the discrete singular convolution element method combined with Taylor series expansion. Keleshteri et al. [17] investigated the nonlinear free and forced vibration behavior of FGP beams by utilizing the harmonic balance and multiscale methods. Chen et al. [18] examined the free and forced vibrations of FGP beams by using the Ritz method and the Newmark-β method. However, despite the significant achievements of these theories and methods, they still have limitations. The aforementioned studies have assumed that there is no energy loss during the vibration process and have neglected the viscoelasticity of the material.

In particular, FG materials often exhibit viscoelastic properties, which are frequently neglected in most existing studies. Viscoelasticity refers to the material's ability to exhibit both elastic deformation and time-dependent viscous behavior when subjected to force [19–21]. This property can have a significant impact on dynamic analysis. For example, when FG beams are subjected to high-frequency or long-term loads, viscoelastic effects can lead to changes in energy dissipation and damping behavior. These changes can directly affect the vibration frequency, amplitude, and response characteristics of the beam. Therefore, to more accurately predict and control the behavior of FG beams, further research into their viscoelastic properties is particularly necessary. In recent years, some research teams have begun to focus on this issue by introducing viscoelastic models to improve traditional beam theory. These models typically employ fractional derivatives [22–24], generalized Kelvin models [25–27], or other advanced mathematical tools to describe the dynamic behavior of viscoelastic materials. Such studies not only help enhance the accuracy of theoretical models but also provide more reliable design references for engineering applications. The adoption of fractional-order models offers significant advantages, as they can describe the characteristics of viscoelastic materials with fewer parameters over a wide range of frequencies [28,29]. Moreover, scholars have experimentally verified that fractional-order models fit the material's experimental curves better than integer-order models [30,31]. Loghman et al. [32] investigated the nonlinear free and forced vibrations of a viscoelastic FG material microbeam modeled by using the finite difference method (FDM) and the finite element method. Taşkin et al. [33] investigated the effect of porosity distribution on vibration and damping behavior of an FG curved beam with a fractional derivative viscoelastic core by using the generalized differential quadrature method (GDQM). Abu-Alshaikh et al. [34] used the Laplace transform method to study the forced vibration response of fractional-order viscoelastic FG beams under moving loads. Fractional differential equations can effectively describe the viscoelastic vibration problem of functionally graded porous beams, but solving these equations still poses challenges. Although previous literature has solved the equations using various methods [32,33], the solution process is often complicated and requires numerical iterative solutions. The main contribution of this work is the proposal of a method based on Bernstein polynomials for directly solving fractional vibration differ-

ential equations in the time domain, thereby avoiding the complex iterative procedures required by traditional methods. The research results show that the method can predict the vibration performance of viscoelastic functionally graded beams under different boundary conditions and various gradient distributions.

2. Viscoelastic Functionally Graded Porous Beam

A viscoelastic FGP beam is considered to comprise length L, width b, and thickness h, as shown in Figure 1. A Cartesian coordinate system (x, z) is introduced, with origin O located at the left end of the midline of the viscoelastic FGP beam, where x and z axes are chosen along the length and thickness directions of the viscoelastic FGP beam, respectively. Four types of porosity distributions along the z-direction are shown in Figure 2 [18]. The first porosity distribution is a uniform distribution. The second porosity distribution is symmetric with the maximum values of Young's modulus and mass density on the top ($z = h/2$) and bottom ($z = -h/2$) surfaces, as well as the minimum values on the midplane ($z = 0$). The third porosity distribution is symmetric with the maximum values of Young's modulus and mass density on the mid-plane, as well as the minimum values on the top and bottom surfaces. The fourth porosity distribution is asymmetric with the maximum values of Young's modulus and mass density, as well as the minimum values on the bottom surface. The effective Young's modulus $E(z)$ and material density $\rho(z)$ of the viscoelastic FGP beam at any depth (z) can be calculated as follows:

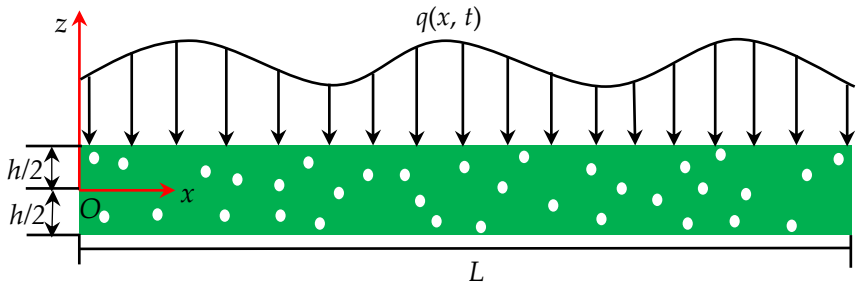


Figure 1. Schematic plot of a fractional, viscoelastic FGP beam.

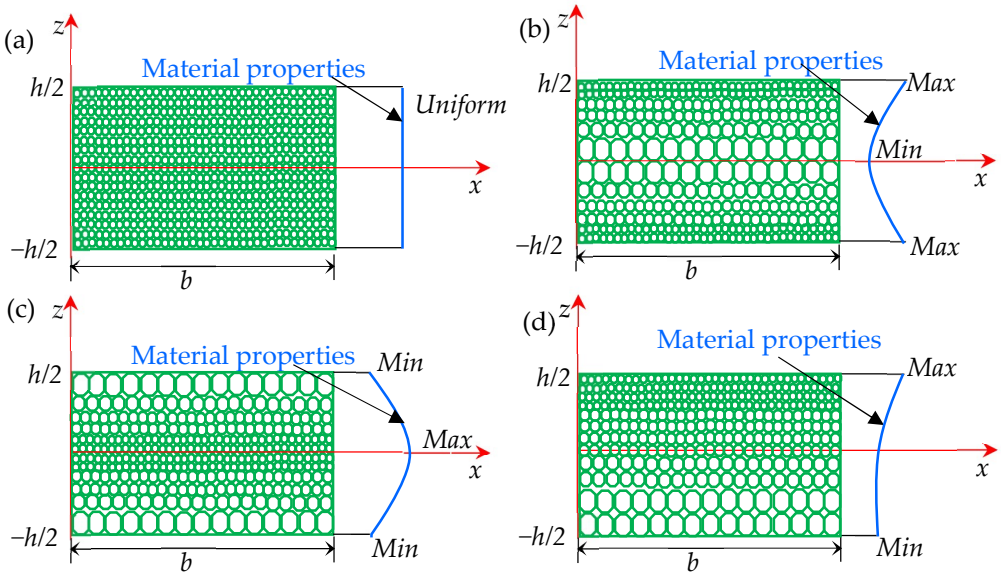


Figure 2. Sketch map of four different types of porosity distribution: (**a**) Type 1, (**b**) Type 2, (**c**) Type 3, and (**d**) Type 4.

Type 1: Uniform porosity distribution

$$E(z) = E_{max}\left(\frac{2}{\pi}\sqrt{1-e_0} - \frac{2}{\pi} + 1\right)^2 \tag{1}$$

$$\rho(z) = \rho_{max}\left(\frac{2}{\pi}\sqrt{1-e_m} - \frac{2}{\pi} + 1\right)^2 \tag{2}$$

Type 2: Symmetric porosity distribution (stiffening in the surface beams)

$$E(z) = E_{max}\left(1 - e_0\cos\left(\frac{\pi z}{h}\right)\right) \tag{3}$$

$$\rho(z) = \rho_{max}\left(1 - e_m\cos\left(\frac{\pi z}{h}\right)\right) \tag{4}$$

Type 3: Symmetric porosity distribution (softening in the surface beams)

$$E(z) = E_{max}\left(1 - e_0\left(\cos\left(\left|\frac{\pi z}{h}\right| - \frac{\pi}{2}\right)\right)\right) \tag{5}$$

$$\rho(z) = \rho_{max}\left(1 - e_m\left(\cos\left(\left|\frac{\pi z}{h}\right| - \frac{\pi}{2}\right)\right)\right) \tag{6}$$

Type 4: Non-symmetric porosity distribution

$$E(z) = E_{max}\left(1 - e_0\cos\left(\frac{\pi z}{2h} + \frac{\pi}{4}\right)\right) \tag{7}$$

$$\rho(z) = \rho_{max}\left(1 - e_m\cos\left(\frac{\pi z}{2h} + \frac{\pi}{4}\right)\right) \tag{8}$$

where E_{max} and $\rho_{\max}$ denote the maximum values of Young's modulus and mass density. e_0 and $e_m = 1 - \sqrt{1-e_0}$ indicate the porosity parameters and mass density, respectively.

3. Theoretical Formulation

3.1. Basic Equations

Within the framework of the Euler–Bernoulli beam theory, the displacement of the viscoelastic FGP beams is defined below:

$$u(x,z,t) = -(z-z_0)\frac{\partial w(x,t)}{\partial x} \tag{9}$$

where t denotes time, while u and w are the displacements of the viscoelastic FGP beam in the x and z directions, respectively.

The physical neutral plane ($z = z_0$) of the viscoelastic FGP beam can be expressed as

$$z_0 = \frac{\int_{-\frac{h}{2}}^{\frac{h}{2}} zE(z)dz}{\int_{-\frac{h}{2}}^{\frac{h}{2}} E(z)dz} \tag{10}$$

According to the assumption of small deformation, the linear strain–displacement relationship of the beam can be expressed as

$$\varepsilon_{xx} = \frac{\partial u}{\partial x} = -(z-z_0)\frac{\partial^2 w(x,t)}{\partial x^2} \tag{11}$$

where ε_{xx} is the strain. The Kelvin–Voigt fractional derivative stress-strain relation for the viscoelastic FGP beam can be written as

$$\sigma_{xx} = E(z)(\varepsilon_{xx} + \eta D_t^{\alpha} \varepsilon_{xx}) \tag{12}$$

where η denotes the viscoelastic coefficient. D^{α} is the Caputo fractional derivative operator, which is defined as

$$D^{\alpha}(f(t)) = \frac{1}{\Gamma(1-\alpha)} \int_0^t \frac{\dot{f}(\tau)}{(t-\tau)^{\alpha}} d\tau, \qquad 0 < \alpha < 1 \tag{13}$$

where α and Γ are the fractional derivative order and Gamma function, respectively.

The strain energy U of the viscoelastic FGP beam can be written as

$$U = \frac{b}{2} \int_0^L \int_{-h/2}^{h/2} (\sigma_{xx} \varepsilon_{xx}) dz dx = \frac{1}{2} \int_0^L (A_1 + A_2 D_t^{a}) \left(\frac{\partial^2 w(x,t)}{\partial x^2} \right)^2 dx \tag{14}$$

where A_1 and A_2 are stiffness components whose expressions are

$$A_1 = b \int_{-h/2}^{h/2} E(z)(z - z_0)^2 dz \tag{15}$$

$$A_2 = b \int_{-h/2}^{h/2} E(z)\eta(z - z_0)^2 dz \tag{16}$$

The kinetic energy K of the viscoelastic FGP beam is given as

$$K = \frac{b}{2} \int_0^L \int_{-h/2}^{h/2} \rho(z) \left[\left(\frac{\partial w}{\partial t} \right)^2 \right] dz dx = \frac{1}{2} \int_0^L I_1 \left(\frac{\partial w(x,t)}{\partial t} \right)^2 dx \tag{17}$$

where I_1 is the inertia item, which can be determined by

$$I_1 = b \int_{-h/2}^{h/2} \rho(z) b dz \tag{18}$$

The potential energy due to the external loads can be calculated by

$$V = -\int_0^L q(x,t) w(x,t) dx \tag{19}$$

where $q(x,t) = q_0(x) \sin \omega t$ represents the transverse distributed load. is the external excitation force frequency.

The Lagrangian functional of the viscoelastic FGP beam can be expressed as

$$\Pi = K - U - V \tag{20}$$

Substituting Equations (14), (17) and (19) into Equation (20) and applying Hamilton's principle, the result is derived as

$$\int_0^t \delta(U + V - K) dt = 0 \tag{21}$$

Thus, the governing equation of the viscoelastic FGP beam can be written as

$$A_1 \frac{\partial^4 w(x,t)}{\partial x^4} + A_2 D_t^{\alpha} \frac{\partial^4 w(x,t)}{\partial x^4} + I_1 \frac{\partial^2 w(x,t)}{\partial t^2} = q(x,t) \tag{22}$$

The moment M_x of a viscoelastic FGP beam is given by

$$\begin{aligned} M_x &= b\int_{-h/2}^{h/2}(z-z_0)\sigma_{xx}dz = b\int_{-h/2}^{h/2}(z-z_0)E(z)(\varepsilon_{xx}+\eta D_t^{\alpha}\varepsilon_{xx})dz \\ &= -A_1\frac{\partial^2 w(x,t)}{\partial x^2} - A_2 D_t^{\alpha}\frac{\partial^2 w(x,t)}{\partial x^2} \end{aligned} \tag{23}$$

The transverse forces Q_{xz} of a viscoelastic FGP beam is given by

$$Q_{xz} = -\frac{\partial M_x}{\partial x} = A_1\frac{\partial^3 w(x,t)}{\partial x^2} + A_2 D_t^{\alpha}\frac{\partial^3 w(x,t)}{\partial x^2} \tag{24}$$

In this study, four types of boundary conditions for viscoelastic FGP beams are considered: clamped–clamped (C-C), clamped–hinged-supported (C-H), hinged–hinged-supported (H-H), and clamped–Free (C-F). The four types of boundary conditions can be defined as

$$\text{(C-C)}: w(0,t) = \frac{\partial w(0,t)}{\partial x} = w(L,t) = \frac{\partial w(L,t)}{\partial x} = 0 \tag{25}$$

$$\text{(C-H)}: w(0,t) = \frac{\partial w(0,t)}{\partial x} = w(L,t) = M_x(L,t) = 0 \tag{26}$$

$$\text{(H-H)}: w(0,t) = M_x(0,t) = w(L,t) = M_x(L,t) = 0 \tag{27}$$

$$\text{(C-F)}: w(0,t) = \frac{\partial w(0,t)}{\partial x} = M_x(L,t) = Q_{xz}(L,t) = 0 \tag{28}$$

Substituting Equations (23) and (24) into Equations (26)–(28) yields

$$\begin{aligned} \text{(C-H)}: \quad & w(0,t) = \tfrac{\partial w(0,t)}{\partial x} = 0 \\ & w(L,t) = A_1\tfrac{\partial^2 w(L,t)}{\partial x^2} + A_2 D_t^{\alpha}\tfrac{\partial^2 w(L,t)}{\partial x^2} = 0 \end{aligned} \tag{29}$$

$$\begin{aligned} \text{(H-H)}: \quad & w(0,t) = A_1\tfrac{\partial^2 w(0,t)}{\partial x^2} + A_2 D_t^{\alpha}\tfrac{\partial^2 w(0,t)}{\partial x^2} = 0 \\ & w(L,t) = A_1\tfrac{\partial^2 w(L,t)}{\partial x^2} + A_2 D_t^{\alpha}\tfrac{\partial^2 w(L,t)}{\partial x^2} = 0 \end{aligned} \tag{30}$$

$$\begin{aligned} \text{(C-F)}: \quad & w(0,t) = \tfrac{\partial w(0,t)}{\partial x} = 0, A_1\tfrac{\partial^2 w(L,t)}{\partial x^2} + A_2 D_t^{\alpha}\tfrac{\partial^2 w(L,t)}{\partial x^2} = 0 \\ & A_1\tfrac{\partial^3 w(L,t)}{\partial x^2} + A_2 D_t^{\alpha}\tfrac{\partial^3 w(L,t)}{\partial x^2} = 0 \end{aligned} \tag{31}$$

In addition, the initial condition is written as

$$w(x,0) = \frac{\partial w(x,0)}{\partial t} = 0 \tag{32}$$

3.2. Bernstein Polynomial Method

In this paper, the Bernstein polynomial method is adopted to solve the governing equation of the fractional viscoelastic FGP beam. Therefore, the transverse displacements $w(x,t)$ of the beam can be expressed as

$$\begin{aligned} w(x,t) &= \lim_{n\to\infty}\sum_{j=0}^{N}\left(\sum_{i=0}^{N} c_i B_{N,i}(x)\right)k_j B_{N,j}(t) \\ &\approx \sum_{j=0}^{N}\sum_{i=0}^{N} B_{N,i}(x)c_i k_j B_{N,j}(t) \end{aligned} \tag{33}$$

where N is the degree of the Bernstein polynomials, c_i and k_j are the correlation coefficients that are related to the degree N in the Bernstein polynomials method, and $B_{N,i}(x)$ and

$B_{N,j}(t)$ denote functions of the Bernstein polynomials. For the N order, the Bernstein polynomial in [0, 1] is

$$B_{N,i}(t) = \binom{N}{i} t^i (1-t)^{N-i} \tag{34}$$

where $\binom{N}{i}$ is the correction coefficient in the Bernstein polynomial, which is used to adjust the influence weights of different control points. The specific expression is

$$\binom{N}{i} = \frac{N!}{i!(N-i)!} \tag{35}$$

Based on the binomial expansion principle, $B_{N,i}(x)$ and $B_{N,j}(t)$ could be expressed as

$$B_{N,i}(x) = \sum_{p=0}^{N-i} (-1)^p \binom{N}{i} \binom{N-i}{p} \frac{1}{L^{i+p}} x^{i+p} \qquad (i = 0, 1, 2, 3, \ldots N) \tag{36}$$

$$B_{N,j}(t) = \sum_{p=0}^{N-j} (-1)^p \binom{N}{j} \binom{N-j}{p} \frac{1}{T_t^{j+p}} t^{j+p} \qquad (j = 0, 1, 2, 3, \ldots N) \tag{37}$$

where T_t is the total time of external load action.

$$\begin{aligned} \mathbf{\Phi}(x) &= [B_{N,0}(x), B_{N,1}(x), B_{N,2}(x), \ldots.., B_{N,N}(x)]^T \\ \mathbf{\Phi}(t) &= [B_{N,0}(t), B_{N,1}(t), B_{N,2}(t), \ldots.., B_{N,N}(t)]^T \end{aligned} \tag{38}$$

The matrix form of Equation (38) is

$$\begin{aligned} \mathbf{\Phi}(x) &= \mathbf{A}\mathbf{T}_n(x) \\ \mathbf{\Phi}(t) &= \mathbf{\Lambda}\mathbf{T}_n(t) \end{aligned} \tag{39}$$

where

$$A_{ij} = \begin{cases} \frac{(-1)^{j-i}\binom{N}{i}\binom{N-i}{j-i}}{L^j}, j \geq i \\ 0, j < i \end{cases} \qquad (i, j = 0, 1, 2, 3, \ldots N) \tag{40}$$

$$\Lambda_{i,j} = \begin{cases} \frac{(-1)^{j-i}\binom{N}{i}\binom{N-i}{j-i}}{T_t^j}, j \geq i \\ 0, j < i \end{cases} \qquad (i, j = 0, 1, 2, 3, \ldots N) \tag{41}$$

$$\begin{aligned} \mathbf{T}_n(x) &= \left[1, x, x^2, \ldots, x^N\right]^T \\ \mathbf{T}_n(t) &= \left[1, t, t^2, \ldots, t^N\right]^T \end{aligned} \tag{42}$$

Substituting Equations (38) and (39) into Equation (33), the transverse displacement w can be expressed as

$$w(x, t) \approx \mathbf{\Phi}^T(x) \mathbf{W} \mathbf{\Phi}(t) \tag{43}$$

where W_{ij} (i, j = 0, 1, …, N) is the undetermined coefficient and can be expressed as

$$\mathbf{W} = \begin{bmatrix} W_{00} & W_{01} & \ldots & W_{0N} \\ W_{10} & W_{11} & \ldots & W_{1N} \\ \vdots & \vdots & \ldots & \vdots \\ W_{N0} & W_{N1} & \ldots & W_{NN} \end{bmatrix} \tag{44}$$

Based on Bernstein polynomials, $\mathrm{D}_t^{\alpha} w(x,t)$ is expressed in matrix form of

$$\begin{aligned}
&\mathrm{D}_t^{\alpha} w(x,t) \cong \mathrm{D}_t^{\alpha} \boldsymbol{\Phi}^{\mathrm{T}}(x) \mathbf{W} \boldsymbol{\Phi}(t) \\
&= \boldsymbol{\Phi}^{\mathrm{T}}(x) \mathbf{W} \boldsymbol{\Lambda} \mathrm{D}_t^{\alpha} \mathbf{T}_N(t) = \boldsymbol{\Phi}^{\mathrm{T}}(x) \mathbf{W} \boldsymbol{\Lambda} \mathbf{D}_t^{\alpha} \left[1, t, \ldots, t^N\right]^{\mathrm{T}} \\
&= \boldsymbol{\Phi}^{\mathrm{T}}(x) \mathbf{W} \boldsymbol{\Lambda} \begin{bmatrix} 0 & 0 & \cdots & 0 \\ 0 & \frac{\Gamma(2)}{\Gamma(2-\alpha)} t^{-\alpha} & \cdots & 0 \\ \vdots & \vdots & \ddots & \vdots \\ 0 & 0 & \cdots & \frac{\Gamma(N+1)}{\Gamma(N+1-\alpha)} t^{-\alpha} \end{bmatrix} \begin{bmatrix} 1 \\ t \\ \vdots \\ t^N \end{bmatrix} \\
&= \boldsymbol{\Phi}^{\mathrm{T}}(x) \mathbf{W} \boldsymbol{\Lambda} \boldsymbol{\Theta} \mathbf{T}_N(t) = \boldsymbol{\Phi}^{\mathrm{T}}(x) \mathbf{W} \boldsymbol{\Lambda} \boldsymbol{\Theta} \boldsymbol{\Lambda}^{-1} \boldsymbol{\Phi}(t) \\
&= \boldsymbol{\Phi}^{\mathrm{T}}(x) \mathbf{W} \mathbf{P} \boldsymbol{\Phi}(t)
\end{aligned} \tag{45}$$

where

$$\mathbf{P} = \boldsymbol{\Lambda} \boldsymbol{\Theta} \boldsymbol{\Lambda}^{-1} \tag{46}$$

$$\boldsymbol{\Theta} = \begin{bmatrix} 0 & 0 & \cdots & 0 \\ 0 & \frac{\Gamma(2)}{\Gamma(2-\alpha)} t^{-\alpha} & \cdots & 0 \\ \vdots & \vdots & \ddots & \vdots \\ 0 & 0 & \cdots & \frac{\Gamma(N+1)}{\Gamma(N+1-\alpha)} t^{-\alpha} \end{bmatrix} \tag{47}$$

Substituting Equation (43) into Equation (22), the governing equation of the viscoelastic FGP beam can be expressed as

$$A_1 \boldsymbol{\Phi}^T(x) \left(\mathbf{G}^T\right)^4 \mathbf{W} \boldsymbol{\Phi}(t) + A_2 \boldsymbol{\Phi}^T(x) \left(\mathbf{G}^T\right)^4 \mathbf{W} \mathbf{P} \boldsymbol{\Phi}(t) + I_1 \boldsymbol{\Phi}^T(x) \mathbf{W} \boldsymbol{\Psi}^2 \boldsymbol{\Phi}(t) = q(x,t) \tag{48}$$

where $\mathbf{G} = \mathbf{A} \mathbf{V} \mathbf{A}^{-1}$ and $\boldsymbol{\Psi} = \boldsymbol{\Lambda} \mathbf{V} \boldsymbol{\Lambda}^{-1}$ are the first-order differential operator matrix of the Bernstein polynomial. $\mathbf{V}$ and $\boldsymbol{\Theta}$ can be written as

$$\mathbf{V} = \left[v_{i,j}\right]_{i,j=0}^{N}, v_{i,j} = \begin{cases} i, i = j+1 \\ 0, i \neq j+1 \end{cases} \tag{49}$$

Substituting Equation (43) into Equations (25) and (29)–(31), four types of boundary conditions can be written in the form of a matrix as follows:

$$\begin{aligned}
\text{(C-H)}: \quad & \boldsymbol{\Phi}^T(0) \mathbf{W} \boldsymbol{\Phi}(t) = \boldsymbol{\Phi}^T(0) \mathbf{G}^T \mathbf{W} \boldsymbol{\Phi}(t) = 0 \\
& \boldsymbol{\Phi}^T(L) \mathbf{W} \boldsymbol{\Phi}(t) = A_1 \boldsymbol{\Phi}^T(L) \left(\mathbf{G}^T\right)^2 \mathbf{W} \boldsymbol{\Phi}(t) + A_2 \boldsymbol{\Phi}^T(L) \left(\mathbf{G}^T\right)^2 \mathbf{W} \mathbf{P} \boldsymbol{\Phi}(t) = 0
\end{aligned} \tag{50}$$

$$\begin{aligned}
\text{(C-C)}: \quad & \boldsymbol{\Phi}^T(0) \mathbf{W} \boldsymbol{\Phi}(t) = \boldsymbol{\Phi}^T(0) \mathbf{G}^T \mathbf{W} \boldsymbol{\Phi}(t) = 0 \\
& \boldsymbol{\Phi}^T(L) \mathbf{W} \boldsymbol{\Phi}(t) = \Phi^T(L) \mathbf{G}^T \mathbf{W} \boldsymbol{\Phi}(t) = 0
\end{aligned} \tag{51}$$

$$\begin{aligned}
\text{(H-H)}: \quad & \boldsymbol{\Phi}^T(0) \mathbf{W} \boldsymbol{\Phi}(t) = A_1 \boldsymbol{\Phi}^T(0) \left(\mathbf{G}^T\right)^2 \mathbf{W} \boldsymbol{\Phi}(t) + A_2 \boldsymbol{\Phi}^T(0) \left(\mathbf{G}^T\right)^2 \mathbf{W} \mathbf{P} \boldsymbol{\Phi}(t) = 0 \\
& \boldsymbol{\Phi}^T(L) \mathbf{W} \boldsymbol{\Phi}(t) = A_1 \boldsymbol{\Phi}^T(L) \left(\mathbf{G}^T\right)^2 \mathbf{W} \boldsymbol{\Phi}(t) + A_2 \boldsymbol{\Phi}^T(L) \left(\mathbf{G}^T\right)^2 \mathbf{W} \mathbf{P} \boldsymbol{\Phi}(t) = 0
\end{aligned} \tag{52}$$

$$\begin{aligned}
\text{(C-F)}: \quad & \boldsymbol{\Phi}^T(0) \mathbf{W} \boldsymbol{\Phi}(t) = \boldsymbol{\Phi}^T(0) \mathbf{G}^T \mathbf{W} \boldsymbol{\Phi}(t) = 0 \\
& A_1 \boldsymbol{\Phi}^T(L) \left(\mathbf{G}^T\right)^2 \mathbf{W} \boldsymbol{\Phi}(t) + A_2 \boldsymbol{\Phi}^T(L) \left(\mathbf{G}^T\right)^2 \mathbf{W} \mathbf{P} \boldsymbol{\Phi}(t) = 0 \\
& A_1 \boldsymbol{\Phi}^T(L) \left(\mathbf{G}^T\right)^3 \mathbf{W} \boldsymbol{\Phi}(t) + A_2 \boldsymbol{\Phi}^T(L) \left(\mathbf{G}^T\right)^3 \mathbf{W} \mathbf{P} \boldsymbol{\Phi}(t) = 0
\end{aligned} \tag{53}$$

Substituting Equation (43) into Equation (32), the initial condition can be written in the form of a matrix as follows:

$$\boldsymbol{\Phi}^T(x) \mathbf{W} \boldsymbol{\Phi}(0) = \boldsymbol{\Phi}^T(x) \mathbf{W} \boldsymbol{\Psi} \boldsymbol{\Phi}(0) = 0 \tag{54}$$

Using the collocation method, variable (x, t) is discretized into (x_r, t_s) by taking nodes, and r, s = 1, 2, 3...M. Equations (48) and (50)–(54) are transformed into a set of algebraic equations.

The scale of the linear equation system generated by the collocation method is determined by the number of configuration points M and the number of basis functions N, where the two-dimensional example uses $M \times M$ uniform configuration points. The scale of the final generated system matrix is $(M^2 + 6M) \times N^2$. By applying the singular value decomposition (SVD) method, the values of **W** are solved, and these values are then substituted into Equation (43) to obtain the numerical solution for the displacement of the viscoelastic FGP beam. The built-in SVD function in MATLAB R2022b is employed for singular value decomposition. Therefore, the numerical solution for the forced vibration of the viscoelastic FGP beams can be directly obtained in the time domain without the need for complex iterative solving processes.

4. Results and Discussion

In this section, the stability, robustness, and accuracy of the proposed approach are verified through some examples dealing with the forced vibration of fractional, viscoelastic FGP beams subjected to different boundary conditions. The results obtained are compared with those in the literature. In addition, the effects of the boundary conditions, porosity distribution types, and viscoelastic coefficient are investigated. The material properties and geometric parameters of the fractional, viscoelastic FGP beams are E_{max} = 210 GPa, $\rho_{\max}$ = 7850 kg/m^3, b = 0.1 m, h = 0.1 m, ω = 1 rad/s, α = 0.25, $\eta = 5 \times 10^{-9} s^{\alpha}$, $q_0(x) = 1000 \sin(x)$ kN, and T_t = 10 s [35].

4.1. Convergence

In order to verify the convergence of the present polynomial series solution, Table 1 presents the mid-span (x = 0.5 m) deflections of viscoelastic FGP beams under different boundary conditions. A comparison shows that the accuracy of the results can be effectively improved as N increases, and the convergent results can be achieved with N = 10. Hence, N = 10 is used in all of the following calculations.

Table 1. Convergence of the mid-span deflections of viscoelastic FGP beams with different number of polynomial terms N. (e_0 = 0.5, t = 2 s, L/h =10).

Boundary Condition	Beam Type	Mid-Span Deflections (mm)					
		N = 6	**N = 7**	**N = 8**	**N = 9**	**N = 10**	**N = 11**
C-H	Type 1	2.524	2.145	2.100	2.102	2.096	2.096
	Type 2	2.128	1.733	1.697	1.698	1.694	1.694
	Type 3	2.914	2.544	2.490	2.492	2.486	2.485
	Type 4	2.483	2.100	2.056	2.057	2.052	2.051
C-F	Type 1	22.099	22.720	22.281	22.309	22.322	22.325
	Type 2	17.856	18.358	18.003	18.026	18.036	18.038
	Type 3	26.203	26.940	26.418	26.452	26.467	26.471
	Type 4	21.629	22.237	21.807	21.835	21.847	21.850
C-C	Type 1	0.957	0.987	0.966	0.966	0.964	0.964
	Type 2	0.774	0.797	0.780	0.781	0.779	0.779
	Type 3	1.135	1.170	1.145	1.146	1.143	1.143
	Type 4	0.937	0.966	0.945	0.946	0.944	0.943

Table 1. *Cont.*

Boundary Condition	Beam Type	Mid-Span Deflections (mm)					
		$N = 6$	$N = 7$	$N = 8$	$N = 9$	$N = 10$	$N = 11$
H-H	Type 1	4.755	4.906	4.797	4.799	4.788	4.787
	Type 2	3.842	3.964	3.876	3.878	3.869	3.868
	Type 3	5.638	5.817	5.688	5.690	5.677	5.676
	Type 4	4.654	4.802	4.695	4.697	4.686	4.686

The convergence of vibration responses is examined by calculating the mid-span amplitude of fractional-order viscoelastic beams with varying numbers of collocation nodes ($M \times M$), as depicted in Table 2. It can be observed that the mid-span amplitude remains relatively unaffected by different numbers of collocation nodes. Consequently, a value of $M = 40$ is adopted for all subsequent vibration analyses.

Table 2. Convergence of the mid-span deflections of viscoelastic FGP beams with numbers of collocation nodes $M \times M$. ($e_0 = 0.5$, $t = 2$ s, L/h =10).

Boundary Condition	Beam Type	Mid-Span Deflections (mm)				
		$M \times M = 10 \times 10$	$M \times M = 20 \times 20$	$M \times M = 30 \times 30$	$M \times M = 40 \times 40$	$M \times M = 50 \times 50$
C-H	Type 1	2.093	2.096	2.096	2.096	2.096
	Type 2	1.691	1.694	1.694	1.694	1.694
	Type 3	2.482	2.486	2.486	2.486	2.486
	Type 4	2.049	2.052	2.052	2.052	2.052
C-F	Type 1	22.212	22.243	22.243	22.322	22.321
	Type 2	17.947	17.972	18.035	18.036	18.036
	Type 3	26.337	26.374	26.374	26.467	26.467
	Type 4	21.739	21.770	21.770	21.847	21.847
C-C	Type 1	0.963	0.964	0.964	0.964	0.964
	Type 2	0.778	0.779	0.779	0.779	0.779
	Type 3	1.142	1.143	1.143	1.143	1.143
	Type 4	0.942	0.944	0.944	0.944	0.944
H-H	Type 1	4.781	4.788	4.788	4.788	4.788
	Type 2	3.863	3.869	3.869	3.869	3.869
	Type 3	5.669	5.677	5.677	5.677	5.677
	Type 4	4.680	4.686	4.686	4.686	4.686

4.2. Validation

To verify the accuracy and effectiveness of the present method, error estimation was conducted between the numerical solution and the analytical solution. The following dimensionless equation serves as a mathematical example

$$\frac{\partial^4 w(x,t)}{\partial x^4} + D_t^{\alpha} \frac{\partial^4 w(x,t)}{\partial x^4} + \frac{\partial^2 w(x,t)}{\partial t^2} = q(x,t) \tag{55}$$

where $x \in [0,1]$, $t \in [0,1]$.

The boundary conditions are

$$\begin{array}{c} w(0,t) = w(1,t) = 0 \\ \frac{\partial w(0,t)}{\partial x} = \frac{\partial w(1,t)}{\partial x} = 0 \end{array} \tag{56}$$

The initial conditions are

$$w(x,0) = \frac{\partial w(x,0)}{\partial t} = 0 \tag{57}$$

Since it is not possible to solve Equation (50) analytically, we instead solve a special case. Assuming there is an analytical solution for Equation (50), it is

$$w(x,t) = x^2(1-x^2)t^2 \tag{58}$$

Substituting Equation (53) into Equation (50), the following equation can be obtained

$$q(x,t) = 2x^2(1-x)^2 + 24t^2 + 24\frac{\Gamma(3)}{\Gamma(2.36)}t^{1.36} \tag{59}$$

In other words, when the transverse distributed load is Equation (59), the corresponding analytical solution is Equation (58). The numerical solution for Equation (55) was also obtained using the method presented in this paper for the same transverse distributed load and compared with the analytical solution. Figure 3 shows the displacement–time curves at different positions of the beam and Figure 4 illustrates the deformation of the beam at different times. It can be seen from the figures that the computational results of the proposed numerical method agree well with the analytical solutions. Therefore, this numerical method is suitable for solving the governing equations of fractional-order, functionally graded beams.

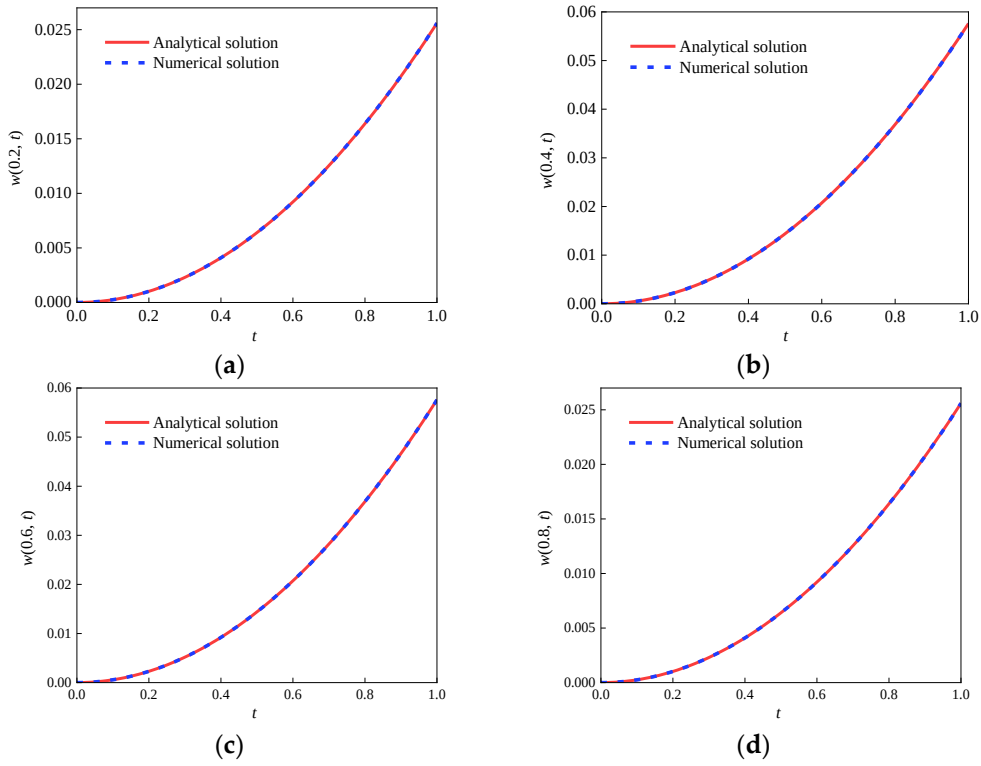


Figure 3. The numerical and analytical solutions of Equation (47) at different positions: (**a**) $x = 0.2$, (**b**) $x = 0.4$, (**c**) $x = 0.6$, (**d**) $x = 0.8$.

Figure 5 compares the mid-span deflections of the viscoelastic beams under the H-H boundary condition with those in the previous reference [36]. The geometric and material parameters are $E = 50.4$ MPa, $\rho = 8180$ kg/m^3, $b = 0.01$ m, $h = 0.01$ m, $L = 1$ m, $T_t = 10$ s, $\omega = 0.5$ rad/s, $\alpha = 0.64$, and $\eta = 0.0045$. The solutions obtained using the present method are in excellent agreement with those derived from previous results for viscoelastic beams.

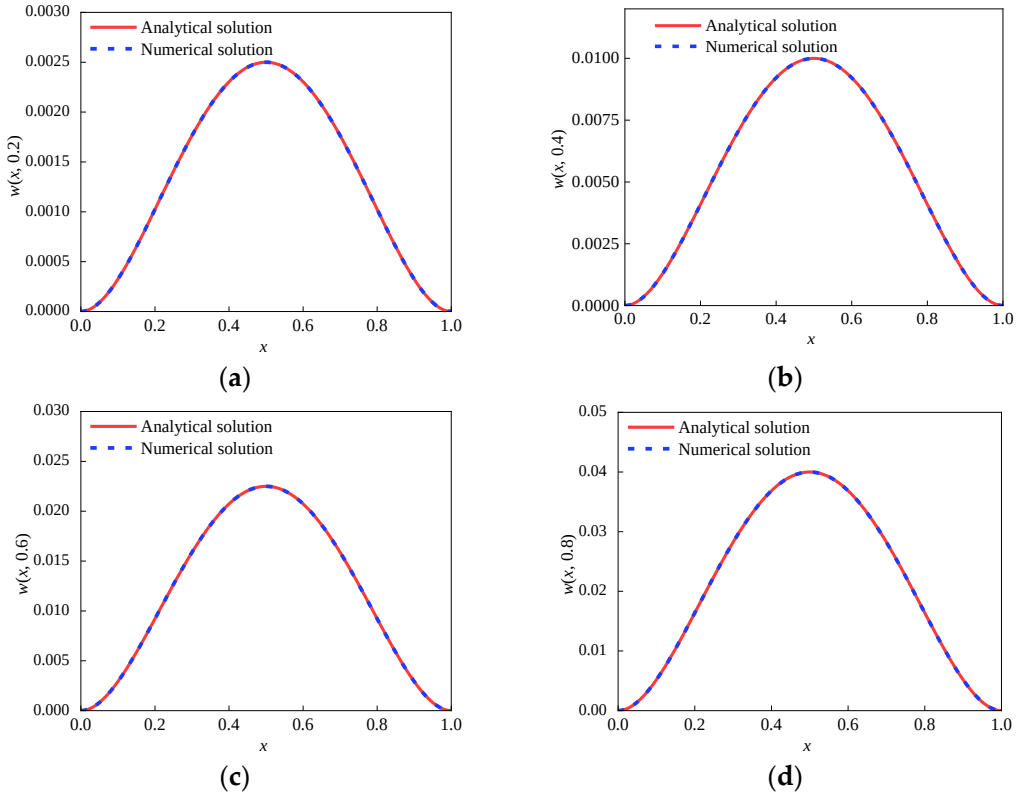


Figure 4. The numerical and analytical solutions of Equation (47) at different times: (**a**) t = 0.2, (**b**) t = 0.4, (**c**) t = 0.6, (**d**) t = 0.8.

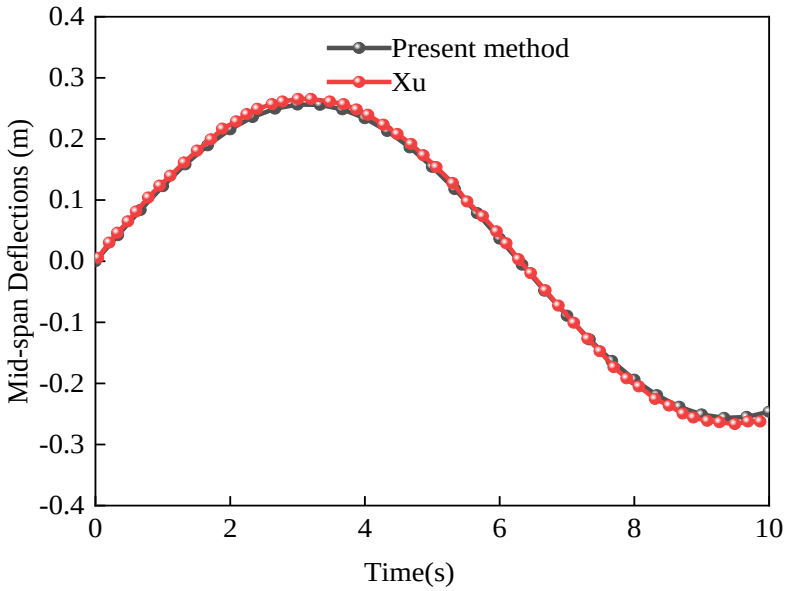
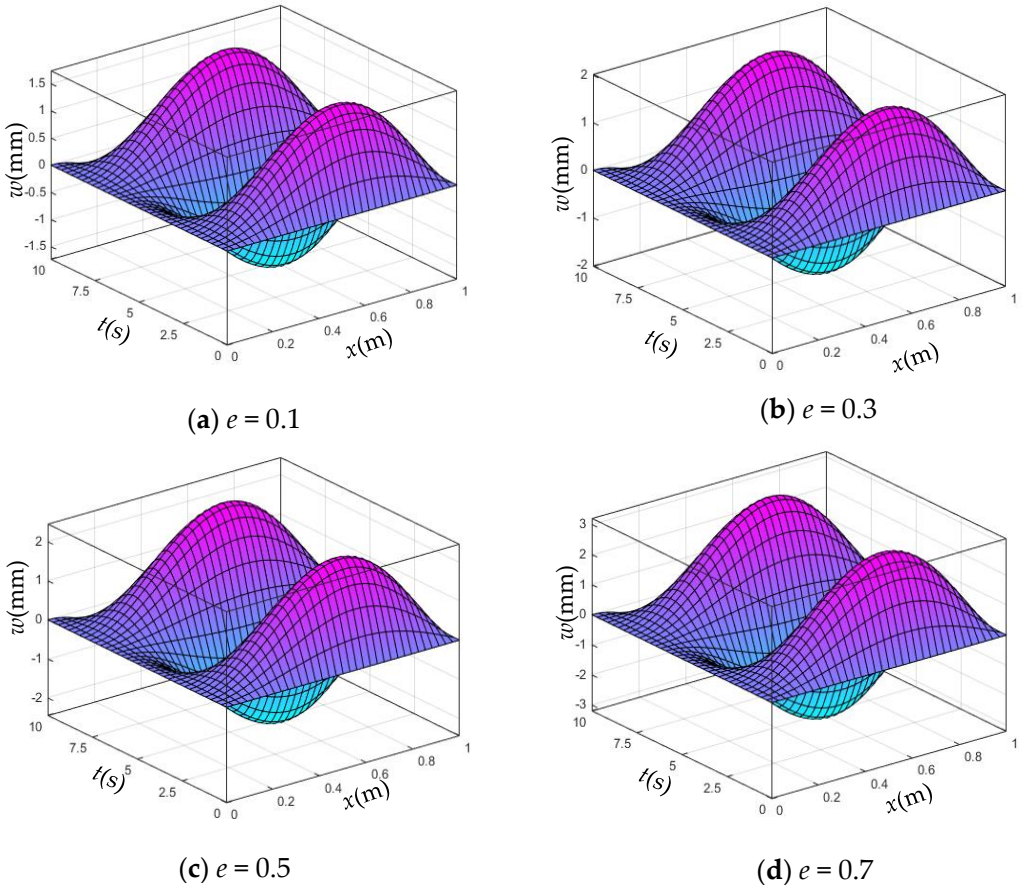


Figure 5. Comparison of mid-span deflection of the viscoelastic beams under the H-H boundary condition [36].

4.3. Parametric Study

Figures 6 and 7 show the influence of porosity on the deflections of viscoelastic FGP beams. It can be observed that the deflections of viscoelastic FGP beams increase as the porosity increases. For the viscoelastic FGP beam with Type 1 porosity distribution under the C-H boundary condition, when the porosity increases from 0 to 0.3, the deflection of the beam significantly increases by 24.6%. As the porosity continues to increase to 0.6, the deflection further rises by 36.8%. When the porosity reaches 0.8, the deflection increase

reaches 39.7%. This phenomenon can be attributed to the reduction in the effective elastic modulus of the material due to increased porosity, which leads to greater deformation of the beam under the same loading conditions. In addition, it is observed from Figure 7 that the deflections of viscoelastic FGP beams with T2 type porosity distribution change linearly, while those of viscoelastic FGP beams with T1, T3, and T4 type porosity distributions change nonlinearly for all boundary conditions. At the same porosity, the T3 type porosity distribution has the greatest effect on the deflection of viscoelastic FGP beams, while the T2 type porosity distribution has the least effect. Specifically, under the C-H boundary condition, when the porosity is 0.2, the deflection of the beam with Type 3 porosity distribution is 12.6% greater than that of the beam with Type 2 porosity distribution. When the porosity rises to 0.5, this difference expands to 46.7%. Notably, when the porosity reaches 0.8, the deflection of the beam with Type 3 porosity distribution is 42.1% higher than that of the beam with Type 2 porosity distribution. This finding is of great importance for optimizing the design of viscoelastic FGP beams and improving their mechanical performance, especially in applications where deformation needs to be strictly controlled, such as aerospace, precision machinery, and civil engineering.



(**a**) $e = 0.1$ (**b**) $e = 0.3$

(**c**) $e = 0.5$ (**d**) $e = 0.7$

Figure 6. Effect of porosity coefficient on the deflections of fractional-order, viscoelastic FGP beams with Type 1 under the C-H boundary condition ($L/h = 10$).

Figures 8 and 9 illustrate the influence of aspect ratio (L/h) on the deflections of viscoelastic FGP beams. It can be seen that the deflection of the viscoelastic FGP beams increases with the increase in aspect ratio. Specifically, when the aspect ratio of a viscoelastic FGP beam increases, its ability to resist deformation weakens, resulting in a significant increase in deflection. In addition, it can be observed from Figure 9 that the deflection value is the greatest when the boundary condition is C-F, whereas it is the smallest when the boundary condition is C-C. This result can be explained from a physical perspective. Under

the C-F boundary condition, one end of the beam is completely fixed and cannot move or rotate, while the other end is completely free and has no constraints. This asymmetrical boundary condition allows the beam to undergo significant displacement under load, resulting in maximum deflection. In contrast, under the C-C boundary condition, both ends of the beam are strictly constrained, and the fixed ends cannot move or rotate, which greatly restricts the deformation capability of the beam, leading to minimum deflection in this case. Additionally, the properties of viscoelastic materials also influence the results. When subjected to force, viscoelastic materials not only undergo immediate elastic deformation but also exhibit gradual viscoelastic deformation over time. This means that under the same external force, the deflection of the viscoelastic FGP beam will gradually increase over time. However, different boundary conditions affect the degree of this deformation. In the C-F boundary condition, since one end is completely free, the overall deformation of the beam is more pronounced, so its deflection increases more significantly over time compared to the C-C boundary condition.

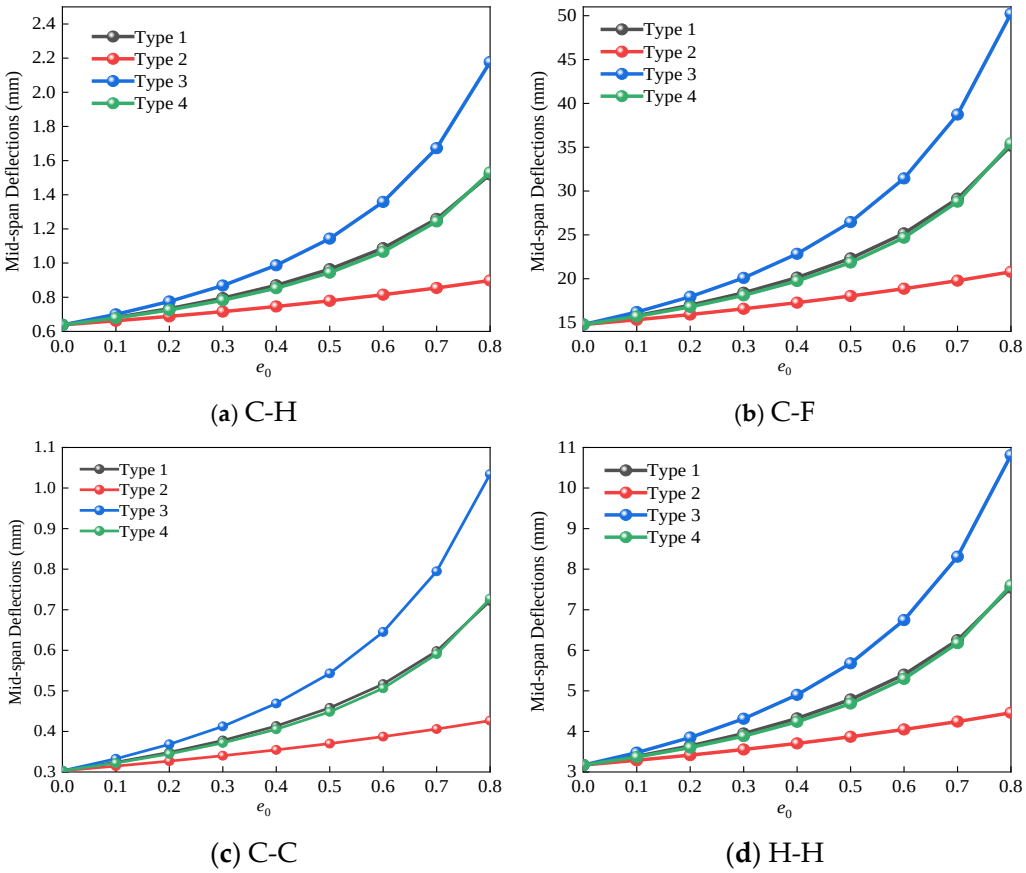
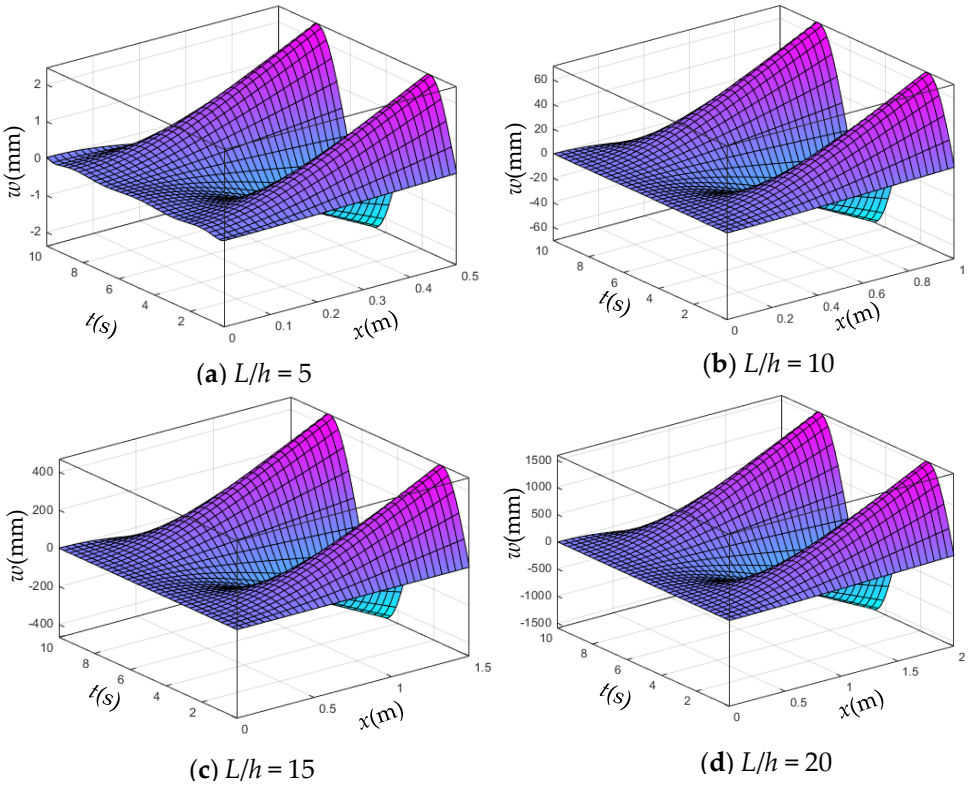


Figure 7. Effect of porosity coefficient on the deflections of fractional-order, viscoelastic FGP beams under different boundary conditions (L/h = 10, t = 2 s).

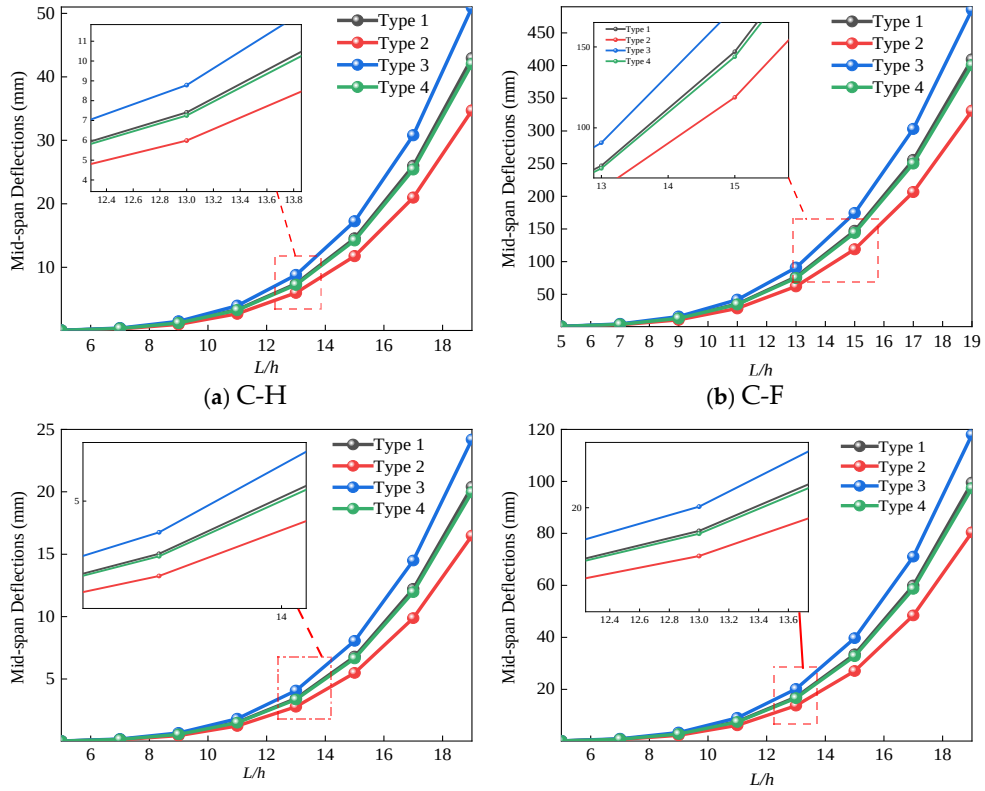
Figure 10 illustrates the influence of viscoelastic coefficients on mid-span deflections of viscoelastic FGP beams. It can be observed that the beam's mid-span deflection gradually decreases as the viscoelastic coefficient increases. When the viscoelastic coefficient increases from 0.003 s^{α} to 0.03 s^{α}, the deflection decreases by 2.3%. However, when it further increases from 0.03 s^{α} to 0.3 s^{α}, the deflection decreases sharply by 19.3%.



(**a**) $L/h = 5$ (**b**) $L/h = 10$

(**c**) $L/h = 15$ (**d**) $L/h = 20$

Figure 8. Effect of aspect ratio on the deflections of fractional-order, viscoelastic FGP beams with Type 1 under the C-F boundary condition ($e = 0.5$).



(**a**) C-H (**b**) C-F

(**c**) C-C (**d**) H-H

Figure 9. Effect of aspect ratio on the deflections of fractional-order, viscoelastic FGP beams under different boundary conditions ($L/h = 10$, $t = 2$ s).

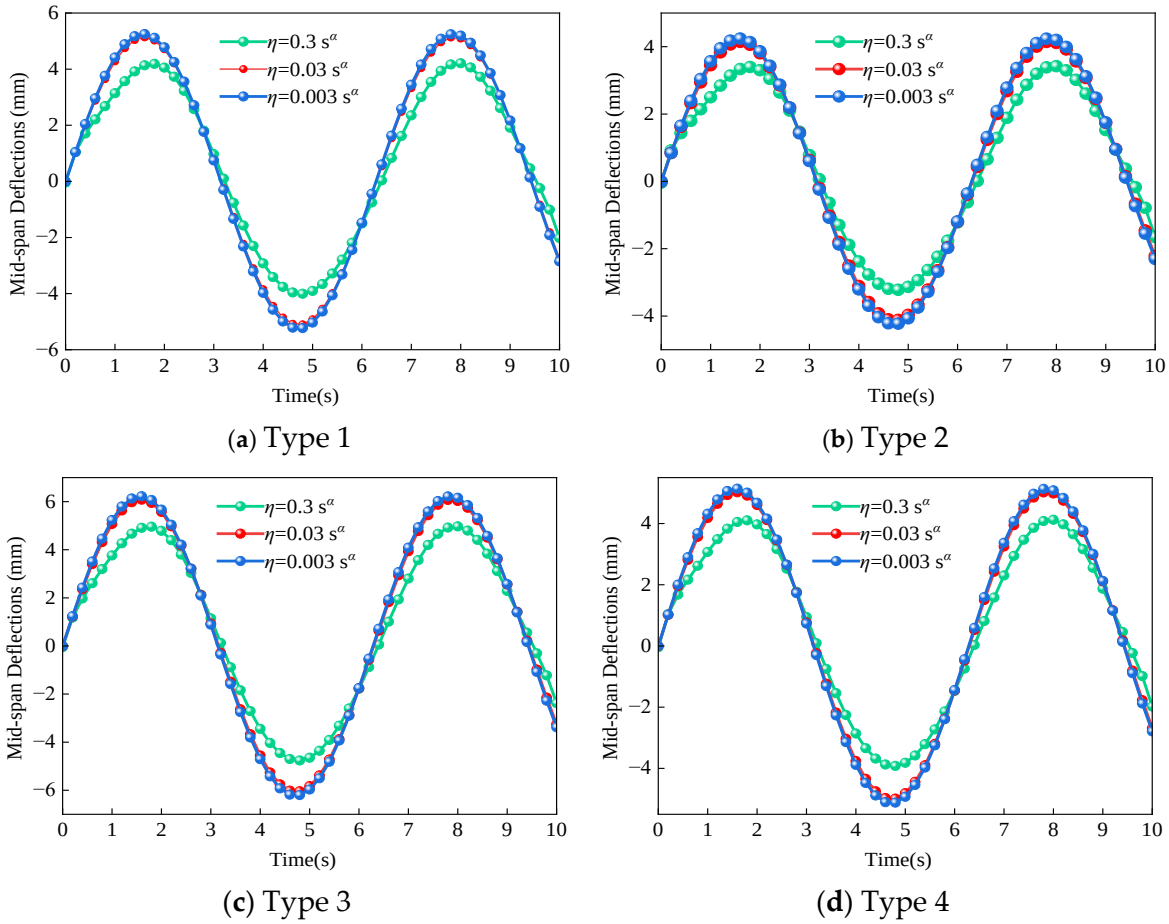


Figure 10. Effect of viscoelastic coefficient on the deflections of fractional-order, viscoelastic FGP beams under the H-H boundary condition (e_0 = 0.5, L/h =10, t = 2 s).

5. Conclusions

Based on the Euler–Bernoulli theory and the Kelvin–Voigt fractional derivative stress-strain relation, the vibration differential equation for viscoelastic FGP beams is established using the Hamilton principle. A method based on Bernstein polynomials is proposed to directly solve fractional vibration, differential equations in the time domain, thereby eliminating the need for complex iterative procedures typical of traditional methods. Some conclusions can be drawn as follows:

(1) The proposed analysis model can effectively analyze the vibration performance of viscoelastic FGP beams. The computational results show that the model has good convergence. Additionally, comparisons with results from previous literature also demonstrate the high computational accuracy of the model.

(2) With the increase in porosity, the mid-span deflection of the viscoelastic FGP beams shows a gradually increasing trend. For the viscoelastic FGP beam with Type 1 porosity distribution under the C-H boundary condition, when the porosity increases from 0 to 0.3, the deflection of the beam significantly increases by 24.6%. As the porosity continues to increase to 0.6, the deflection further rises by 36.8%. When the porosity reaches 0.8, the deflection increase reaches 39.7%. This result indicates that the influence of porosity on the deflection of viscoelastic FGP beams presents a nonlinear characteristic and shows a more significant influence effect within the higher porosity range.

(3) Among the four porosity distribution patterns, the viscoelastic FGP beam with Type 3 porosity distribution exhibits the largest deflection deformation, whereas the beam with Type 2 porosity distribution demonstrates the smallest deflection. This study further

reveals that as porosity increases, the influence of different porosity distribution patterns on the deflection of viscoelastic FGP beams becomes increasingly pronounced. Specifically, under the C-H boundary condition, when the porosity is 0.2, the deflection of the beam with Type 3 porosity distribution is 12.6% greater than that of the beam with Type 2 porosity distribution. When the porosity rises to 0.5, this difference expands to 46.7%. Notably, when the porosity reaches 0.8, the deflection of the beam with Type 3 porosity distribution is 42.1% higher than that of the beam with Type 2 porosity distribution.

(4) With the increase of the viscoelastic coefficient, the mid-span deflection of FGP beams gradually decreases, and the mid-span deflection of FGP beams shows a significant nonlinear attenuation characteristic. When the viscoelastic coefficient increases from 0.003 s^{α} to 0.03 s^{α}, the deflection decreases by 2.3%. However, when it further increases from 0.03 s^{α} to 0.3 s^{α}, the deflection decreases sharply by 19.3%. The nonlinear relationship between the viscoelastic coefficient and deflection can serve as an effective guideline for designing time-varying stiffness structures in fields such as aviation-flexible mechanisms and intelligent vibration-damping devices.

This study investigates the mechanical behavior of viscoelastic FGP beams based on the Euler–Bernoulli beam theory, which disregards the effects of shear deformation. However, for beams with relatively low slenderness ratios, the influence of shear deformation can be substantial, potentially resulting in significant errors in the calculation results derived from the Euler–Bernoulli beam theory. To improve the applicability and accuracy of the theoretical model, the Timoshenko beam theory will be employed to study the vibration characteristics of fractional viscoelastic FGP beams in subsequent research.

Author Contributions: Conceptualization, Y.C.; writing—review and editing, Y.C.; methodology, Y.C. and S.C.; investigation, Y.Y., X.W. and G.X.; data curation, Y.Y., X.W. and G.X.; visualization, X.W., G.X. and S.C.; resources, T.Z. and G.X.; writing—review and editing, T.Z. and G.X.; supervision, T.Z. All authors have read and agreed to the published version of the manuscript.

Funding: The authors would like to thank the National Natural Science Foundation of China (12472135, 12402167), the Guangdong Basic and Applied Basic Research Foundation (2025A1515011352, 2023A1515011073, 2025A1515011759), and the Engineering Technology Research Center of Guangdong Provincial Department of Education (2024GCZX007).

Data Availability Statement: The original contributions presented in this study are included in the article. Further inquiries can be directed to the corresponding author.

Conflicts of Interest: The authors declare no conflicts of interest.

References

1. Wu, H.L.; Yang, J.; Kitipornchai, S. Mechanical analysis of functionally graded porous structures: A review. *Int. J. Struct. Stab. Dyn.* **2020**, *20*, 2041015. [CrossRef]
2. Zhou, K.; Huang, X.C.; Tian, J.J.; Hua, H.X. Vibration and flutter analysis of supersonic porous functionally graded material plates with temperature gradient and resting on elastic foundation. *Compos. Struct.* **2018**, *204*, 63–79. [CrossRef]
3. Jędrysiak, J. Tolerance modelling of free vibrations of medium thickness functionally graded plates. *Compos. Struct.* **2018**, *202*, 1253–1262. [CrossRef]
4. Babaei, M.; Kiarasi, F.; Asemi, K.; Hosseini, M. Functionally graded saturated porous structures: A review. *J. Comput. Appl. Math.* **2022**, *53*, 297–308. [CrossRef]
5. Xu, W.T.; Pan, G.J.; Moradi, Z.; Shafiei, N. Nonlinear forced vibration analysis of functionally graded non-uniform cylindrical microbeams applying the semi-analytical solution. *Compos. Struct.* **2021**, *275*, 114395. [CrossRef]
6. Al Rjoub, Y.S.; Hamad, A.G. Free vibration of functionally Euler-Bernoulli and Timoshenko graded porous beams using the transfer matrix method. *Ksce. J. Civ. Eng.* **2017**, *21*, 792–806. [CrossRef]
7. Chen, D.; Yang, J.; Kitipornchai, S. Nonlinear vibration and post buckling of functionally graded graphene reinforced porous nanocomposite beams. *Compos. Sci. Technol.* **2017**, *142*, 235–245. [CrossRef]

8. Ebrahimi-Nejad, S.; Shaghaghi, G.R.; Miraskari, F. Size-dependent vibration in two-directional functionally graded porous nanobeams under hygro-thermo-mechanical loading. *Eur. Phys. J. Plus* **2019**, *134*, 465. [CrossRef]
9. Noori, A.R.; Aslan, T.A.; Temel, B. Dynamic analysis of functionally graded porous beams using complementary functions method in the Laplace domain. *Compos. Struct.* **2021**, *256*, 113094. [CrossRef]
10. Jędrysiak, J. Theoretical tolerance modelling of dynamics and stability for axially functionally graded (AFG) beams. *Materials* **2023**, *16*, 2096. [CrossRef]
11. Qin, B.; Zhong, R.; Wang, Q.S.; Zhao, X. A Jacobi-Ritz approach for FGP beams with arbitrary boundary conditions based on a higher-order shear deformation theory. *Compos. Struct.* **2020**, *247*, 112435. [CrossRef]
12. Nguyen, N.D.; Nguyen, T.N.; Nguyen, T.K.; Vo, T.P. A new two-variable shear deformation theory for bending, free vibration and buckling analysis of functionally graded porous beams. *Compos. Struct.* **2022**, *282*, 115095. [CrossRef]
13. Esen, I. Dynamic response of functional graded Timoshenko beams in a thermal environment subjected to an accelerating load. *Eur. J. Mech. A-Solids* **2019**, *78*, 103841. [CrossRef]
14. Alnujaie, A.; Akbas, S.D.; Eltaher, M.A.; Assie, A.E. Damped forced vibration analysis of layered functionally graded thick beams with porosity. *Smart Struct. Syst.* **2021**, *27*, 679–689. [CrossRef]
15. Wu, J.; Chen, L.; Wu, R.; Chen, X.C. Nonlinear forced vibration of bidirectional functionally graded porous material beam. *Shock. Vib.* **2021**, *2021*, 6675125. [CrossRef]
16. Lei, Y.L.; Gao, K.; Wang, X.W.; Yang, J. Dynamic behaviors of single-and multi-span functionally graded porous beams with flexible boundary constraints. *Appl. Math. Model.* **2020**, *83*, 754–776. [CrossRef]
17. Keleshteri, M.M.; Jelovica, J. Analytical assessment of nonlinear forced vibration of functionally graded porous higher order hinged beams. *Compos. Struct.* **2022**, *298*, 115994. [CrossRef]
18. Chen, D.; Yang, J.; Kitipornchai, S. Free and forced vibrations of shear deformable functionally graded porous beams. *Int. J. Mech. Sci.* **2016**, *108*, 14–22. [CrossRef]
19. Jalaei, M.H.; Civalek, Ö. On dynamic instability of magnetically embedded viscoelastic porous FG nanobeam. *Int. J. Eng. Sci.* **2019**, *143*, 14–32. [CrossRef]
20. Jalaei, M.H.; Thai, H.T.; Civalek, Ö. On viscoelastic transient response of magnetically imperfect functionally graded nanobeams. *Int. J. Eng. Sci.* **2022**, *172*, 103629. [CrossRef]
21. Pawlus, D. Dynamic behaviour of three-layered annular plates with viscoelastic core under lateral loads. *J. Theor. Appl. Mech.* **2015**, *53*, 775–788. [CrossRef]
22. Zhang, W.; Capilnasiu, A.; Sommer, G.; Holzapfel, G.A.; Nordsletten, D.A. An efficient and accurate method for modeling nonlinear fractional viscoelastic biomaterials. *Comput. Methods Appl. Mech. Eng.* **2020**, *362*, 112834. [CrossRef]
23. Amabili, M.; Balasubramanian, P.; Breslavsky, I. Anisotropic fractional viscoelastic constitutive models for human descending thoracic aortas. *J. Mech. Behav. Biomed. Mater.* **2019**, *99*, 186–197. [CrossRef]
24. Li, X.; Xue, Z.; Tian, X. A modified fractional order generalized bio-thermoelastic theory with temperature-dependent thermal material properties. *Int. J. Therm. Sci.* **2018**, *132*, 249–256. [CrossRef]
25. Ghayesh, M.H. Viscoelastic dynamics of axially FG microbeams. *Int. J. Eng. Sci.* **2019**, *135*, 75–85. [CrossRef]
26. Shariati, A.; Jung, D.W.; Mohammad-Sedighi, H.; Zur, K.K.; Habibi, M.; Safa, M. On the vibrations and stability of moving viscoelastic axially functionally graded nanobeams. *Materials* **2020**, *13*, 1707. [CrossRef] [PubMed]
27. Akbaş, Ş.D.; Fageehi, Y.A.; Assie, A.E.; Eltaher, M.A. Dynamic analysis of viscoelastic functionally graded porous thick beams under pulse load. *Eng. Comput.* **2020**, *27*, 365–377. [CrossRef]
28. Lewandowski, R.; Baum, M. Dynamic characteristics of multilayered beams with viscoelastic layers described by the fractional Zener model. *Arch. Appl. Mech.* **2015**, *85*, 1793–1814. [CrossRef]
29. Zheng, G.Z.; Zhang, N.T.; Lv, S.T. The application of fractional derivative viscoelastic models in the finite element method: Taking several common models as examples. *Fractal. Fract.* **2024**, *8*, 103. [CrossRef]
30. Hu, D.; Zhang, J.; Chen, H. Random flutter analysis of a novel binary airfoil with fractional order viscoelastic constitutive relationship. *Mech. Syst. Signal. Pr.* **2024**, *221*, 111755. [CrossRef]
31. Song, P.; Wei, P.; Zhou, X. Vibration of rectangular plate on fractional order viscoelastic foundation subjected to standing and moving loads. *Mech. Time-Depend. Mat.* **2024**, *28*, 541–561. [CrossRef]
32. Loghman, E.; Kamali, A.; Bakhtiari-Nejad, F.; Abbaszadeh, M. Nonlinear free and forced vibrations of fractional modeled viscoelastic FGM micro-beam. *Appl. Math. Model.* **2021**, *92*, 297–314. [CrossRef]
33. Taşkin, M.; Demir, Ö. Effect of porosity distribution on vibration and damping behavior of inhomogeneous curved sandwich beams with fractional derivative viscoelastic core. *Eng. Comput.* **2023**, *40*, 538–563. [CrossRef]
34. Abu-Alshaikh, I.M.; Almbaidin, A.A. Analytical responses of functionally graded beam under moving mass using Caputo and Caputo–Fabrizio fractional derivative models. *J. Vib. Control* **2020**, *26*, 1859–1867. [CrossRef]

35. Sun, L.; Chen, Y.; Dang, R.; Cheng, G.; Xie, J. Shifted Legendre polynomials algorithm used for the numerical analysis of viscoelastic plate with a fractional order model. *Math. Comput. Simulat.* **2022**, *193*, 190–203. [CrossRef]
36. Xu, J.; Chen, Y.D.; Tai, Y.P.; Xu, X.M.; Shi, G.D.; Chen, N. Vibration analysis of complex fractional viscoelastic beam structures by the wave method. *Int. J. Mech. Sci.* **2020**, *167*, 105204. [CrossRef]

Disclaimer/Publisher's Note: The statements, opinions and data contained in all publications are solely those of the individual author(s) and contributor(s) and not of MDPI and/or the editor(s). MDPI and/or the editor(s) disclaim responsibility for any injury to people or property resulting from any ideas, methods, instructions or products referred to in the content.